Apparent coherence loss in phase space tomography

ZHENGYUN ZHANG,[1,4] CHENGLONG BAO,[2,*] HUI JI,[2] ZUOWEI SHEN,[2] AND GEORGE BARBASTATHIS[1,3]

[1]BioSyM IRG, Singapore-MIT Alliance for Research and Technology (SMART) Centre, 1 CREATE Way, #04-13/14 Enterprise Wing, Singapore 138602, Singapore
[2]Department of Mathematics, National University of Singapore, 10 Lower Kent Ridge Road, Block S17 Level 4, Singapore 119076, Singapore
[3]Department of Mechanical Engineering, Massachusetts Institute of Technology, 77 Massachusetts Avenue, Cambridge, Massachusetts 02139, USA
[4]e-mail: zhengyun@smart.mit.edu
*Corresponding author: matbc@nus.edu.sg

A sensor pixel integrates optical intensity across its extent, and we explore the role that this integration plays in phase space tomography. The literature is inconsistent in its treatment of this integration—some approaches model this integration explicitly, some approaches are ambiguous about whether this integration is taken into account, and still some approaches assume pixel values to be point samples of the optical intensity. We show that making a point-sample assumption results in apodization of and thus systematic error in the recovered ambiguity function, leading to underestimating the overall degree of coherence. We explore the severity of this effect using a Gaussian Schell-model source and discuss when this effect, as opposed to noise, is the dominant source of error in the retrieved state of coherence.   © 2017 Optical Society of America

1. INTRODUCTION

Phase space tomography (PST) is a classic approach for solving the optical coherence retrieval problem, i.e., estimating the state of coherence of an optical field using only measurements of intensity [1–7]. The approach is grounded in the idea that the Fourier transform of intensity profiles captured under varying levels of defocus form slices of the ambiguity function, a phase space representation that quantifies an optical field's state of coherence [8,9].

More specifically, the state of coherence of a quasimonochromatic (i.e., the wavelength range is much smaller than the mean wavelength λ) optical beam can be characterized by the mutual intensity $J(x_1, y_1, x_2, y_2)$ on some reference plane normal to the direction of propagation:

$$J(x_1, y_1, x_2, y_2) = \langle U(x_1, y_1) U^*(x_2, y_2) \rangle,$$

where $\langle \cdot \rangle$ denotes the ensemble average, $U(x, y)$ is the scalar field on this plane and $*$ denotes complex conjugation. The ambiguity function is related to the mutual intensity via a Fourier transform along the two mean position variables x and y:

$$A(f_x, f_y, \xi, \eta) = \iint \breve{J}(x, y, \xi, \eta) \exp[-2\mathrm{j}\pi(x f_x + y f_y)]\mathrm{d}x\mathrm{d}y,$$

where $\breve{J}$ is the mutual intensity written in mean and difference coordinates:

$$\breve{J}(x, y, \xi, \eta) = J(x + \xi/2, y + \eta/2, x - \xi/2, y - \eta/2).$$

Different slices through the origin correspond to the Fourier transform of the transverse intensity profile captured with varying amounts of defocus, astigmatism, and magnification:

$$\iint I_m(u/\mu_m, v/\nu_m) \exp[-\mathrm{j}2\pi(\alpha u + \beta v)]\mathrm{d}u\mathrm{d}v$$
$$= A(\alpha \cos \theta_m, \beta \cos \phi_m, \alpha \sin \theta_m, \beta \sin \phi_m), \quad \textbf{(1)}$$

where parameters $\mu_m > 0$, $\nu_m > 0$, $-\frac{\pi}{2} \leq \theta_m$, and $\phi_m \leq \frac{\pi}{2}$ describe the amount of magnification and (possibly astigmatic) defocus in the imaging system for the mth recorded intensity profile, I_m. By capturing a sufficient number of slices, the ambiguity function, and therefore the mutual intensity, can be reconstructed. These profiles are usually captured via an image sensor, and an estimate for the state of coherence is computed from these images by solving an inverse problem.

An accurate solution to this inverse problem requires an accurate model of how measurements are formed, and one component of this model is the mathematical relationship between the spatial intensity profile and the measured pixel values on the sensor. While one approach in the literature models the pixel value as a noisy measurement of the intensity *integrated* across the extent of the pixel [3], several papers appear to ignore the pixel extent and model the measured values as *point samples* of the true intensity instead [4–6]. Earlier approaches using the inverse Radon transform do not give an explicit expression for continuous intensity profiles in terms of the discrete pixel measurements [1,2]; accounting for the pixel extent in the reconstruction would have required a nontrivial deconvolution step.

While assuming pixel values to be point samples of the intensity would likely result in spatial blurring in standard imaging applications, the same assumption applied to phase space tomography can incidentally *also* lead to underestimating the degree of coherence, undermining the accuracy of the results. In this paper, we explain the mechanism behind this apparent loss of coherence and derive an expression for computing the magnitude of its effect in phase space tomography. As this expression is dependent on both the source and the measurement procedure, we focus on the demonstrative example of a Gaussian Schell-model source to discuss situations where this loss may be significant based on relative pixel size and noise characteristics.

2. BLUR AND COHERENCE

Let us first discuss why spatial blurring would lead to an underestimation of coherence. To do so, we consider a simple intuitive example: the classic two-slit experiment. For quasi-monochromatic light of uniform intensity traversing two slits, the far-field intensity will be a sinusoidal pattern of the following form:

$$I(x) = I_0 + I_1 \cos(2\pi f x + \phi) \geq 0,$$

where the spatial frequency is given by $f = D/(2\lambda z)$ with D being the slit separation, λ being the average wavelength, and z being the propagation distance. The average phase difference between the two slits is given by ϕ, and their degree of coherence is given by the contrast, $0 \leq I_1/I_0 \leq 1$. A contrast of 1 indicates fully coherent light, and a contrast of 0 indicates fully incoherent light. Now suppose we captured this intensity profile with image sensor pixels of width W. Integration across the extent of the pixel prevents the (noiseless) intensity from ever reaching $I_0 + I_1$ or $I_0 - I_1$; it would be as if we were point sampling the intensity of a different sinusoidal pattern with a modified contrast given by

$$\widetilde{I}_1 = I_1 \sin(\pi f W)/(\pi f W).$$

Hence, if we simply interpreted these pixel values as point samples rather than integrated measurements of the intensity profile, we will underestimate the contrast and hence underestimate the degree of coherence. Even with pixel spacing equal to the Nyquist interval, we lose roughly 36% of the contrast if we use full fill-factor pixels. In practice, it is difficult to make the pixel size arbitrarily small to negate this effect—decreasing

the fill factor would result in loss of light and an increase in noise, whereas increasing the pixel density would exacerbate the already large storage costs needed to solve the coherence retrieval inverse problem. Thus, it would be useful to quantify the effect of pixel integration on measurements of coherence conducted via the well-known phase space tomography approach.

3. EFFECT OF PIXEL INTEGRATION IN PST

In phase space tomography, intensity profiles are usually captured with image sensors, and thus application of Eq. (1) implies some reconstruction process to form the continuous intensity profile $I_m(u, v)$ from the discrete samples that image sensors provide. The simplest and fastest approach is to assume that the pixel values correspond to point samples of the continuous intensity profile. However, since the pixel integrates intensity across its extent, this assumption implies that measurements are instead point samples of a blurred intensity profile $\widetilde{I}_m(u, v)$:

$$\widetilde{I}_m(u, v) = \iint I_m(\iota, \zeta) P_m(u - \iota, v - \zeta) d\iota d\zeta,$$

where the pixel kernel $P_m(u, v)$ specifies the sensitivity of the pixel as a function of position. For example, the pixel kernel for an ideal $\Delta \times \Delta$ square pixel would be $\mathrm{rect}(u/\Delta)\mathrm{rect}(v/\Delta)$ scaled by a constant. Without loss of generality, let us assume that $\iint P_m(u/\mu_m, v/\nu_m) du dv = 1$, where μ_m and ν_m are per-slice magnification factors defined earlier.

Thus, by ignoring the pixel kernel and making a point sample assumption, we effectively assume the pixel values to be measurements of an alternate ambiguity function $\widetilde{A}$:

$$\iint \widetilde{I}_m(u/\mu_m, v/\nu_m) \exp[-j2\pi(\alpha u + \beta v)] du dv$$
$$= \widetilde{A}(\alpha \cos \theta_m, \beta \cos \phi_m, \alpha \sin \theta_m, \beta \sin \phi_m),$$

which is related to the true ambiguity function via an apodization function Π:

$$\widetilde{A}(f_x, f_y, \xi, \eta) = A(f_x, f_y, \xi, \eta)\Pi(f_x, f_y, \xi, \eta).$$

The pixel kernel(s) are folded into this apodization function, implying the following properties for Π:

1. any slice through the origin is the Fourier transform of a nonnegative-valued function, i.e., for all $-\frac{\pi}{2} \leq \theta, \phi \leq \frac{\pi}{2}$:

$$\Pi(\alpha \cos \theta, \beta \cos \phi, \alpha \sin \theta, \beta \sin \phi)$$
$$= \iint p(u, v; \theta, \phi) \exp[-j2\pi(\alpha u + \beta v)] du dv,$$

where $p(u, v; \theta, \phi) \geq 0$, $\iint p(u, v; \theta, \phi) du dv = 1$ for all θ, ϕ;

2. $p(u, v; \theta_m, \phi_m) = P_m(u/\mu_m, v/\nu_m)$ for all measurement indices m.

Hence, Π has greatest magnitude at the origin:

$$|\Pi(f_x, f_y, \xi, \eta)| \leq |\Pi(0, 0, 0, 0)| = 1, \qquad \textbf{(2)}$$

due to the nonnegativity of $p(u, v; \theta, \phi)$ as well as normalization, with equality only at the origin. Thus, the apodization function Π causes the magnitude of the alternate ambiguity function $\widetilde{A}$ to have a lower magnitude compared to the true

ambiguity function A as we move away from the origin. In other words, convolution with the nonnegative-valued pixel kernel blurs the images we capture, which is evident in the reduction in magnitude of high frequency components of images taken at various amounts of defocus. For ideal pixels, the magnitude of Π falls off roughly proportional to $1/|\alpha\beta| = [(f_x^2 + \xi^2)(f_y^2 + \eta^2)]^{-1/2}$ due to the denominator of the sinc function for each slice.

Spatial blur induced by pixel integration is of course well known in the standard imaging literature. In phase space tomography, however, this pixel integration additionally reduces the apparent coherence of the optical field, as we will now show using the expression derived above for the alternate ambiguity function. To see this, let us first define the overall degree of coherence for an optical field as [10]

$$\mathcal{M} = \frac{\iint \iint |J(x_1, y_1, x_2, y_2)|^2 dx_1 dy_1 dx_2 dy_2}{\left[\iint J(x, y, x, y) dx dy\right]^2}.$$

This nonnegative quantity corresponds to the concept of purity in quantum mechanics and reaches a maximum value of 1 when the field is fully spatially coherent. For partially coherent fields, $1/\mathcal{M}$ is roughly the number of prominent coherent modes [11] in the source. Since the mutual intensity and ambiguity function form a Fourier transform pair, we can write $\mathcal{M}$ in terms of the ambiguity function as well:

$$\mathcal{M} = \frac{\iint \iint |A(f_x, f_y, \xi, \eta)|^2 df_x df_y d\xi d\eta}{A^2(0, 0, 0, 0)}. \qquad (3)$$

The action of the apodization function thus yields a new $\widetilde{\mathcal{M}}$:

$$\widetilde{\mathcal{M}} = \frac{\iint \iint |\Pi(f_x, f_y, \xi, \eta)A(f_x, f_y, \xi, \eta)|^2 df_x df_y d\xi d\eta}{\Pi^2(0, 0, 0, 0)A^2(0, 0, 0, 0)}. \qquad (4)$$

It is evident from Eq. (2) that $\widetilde{\mathcal{M}} < \mathcal{M}$, except for equality when the ambiguity function is a delta function, i.e., an infinitely wide fully spatially incoherent field. Thus, if we do not consider spatial blur introduced by integration across each pixel, we will think we have a set of measurements corresponding to an alternate apodized ambiguity function $\widetilde{A}$ (or a blurred Wigner distribution) that is less coherent.

Of course, this apodization results in systematic error in the recovered mutual intensity, Wigner distribution, and ambiguity functions; the relative magnitude of this error is given by

$$\mathcal{E} = \left[\frac{\iint \iint |E_J(x_1, x_2, y_1, y_2)|^2 dx_1 dy_1 dx_2 dy_2}{\iint \iint |J(x_1, y_1, x_2, y_2)|^2 dx_1 dy_1 dx_2 dy_2}\right]^{1/2}$$

$$= \left[\frac{\iint \iint |E_A(f_x, f_y, \xi, \eta)|^2 df_x df_y d\xi d\eta}{\iint \iint |A(f_x, f_y, \xi, \eta)|^2 df_x df_y d\xi d\eta}\right]^{1/2}$$

$$= [\widetilde{\mathcal{M}}/\mathcal{M} - 2\,\mathrm{Re}\{\mathcal{M}_{\mathrm{cross}}/\mathcal{M}\} + 1]^{1/2}, \qquad (5)$$

where

$$E_J(x_1, y_1, x_2, y_2) = \widetilde{J}(x_1, y_1, x_2, y_2) - J(x_1, y_1, x_2, y_2)$$

$$E_A(f_x, f_y, \xi, \eta) = \widetilde{A}(f_x, f_y, \xi, \eta) - (f_x, f_y, \xi, \eta)$$

$$\mathcal{M}_{\mathrm{cross}} = \iint \iint |A(f_x, f_y, \xi, \eta)|^2 \Pi(f_x, f_y, \xi, \eta)$$
$$\times df_x df_y d\xi d\eta.$$

The magnitude of the apparent loss in coherence and systematic error depends on both the measurement procedure (which determines Π) and the coherence of the source being measured (described by A), so we will consider the demonstrative example of a one-dimensional Gaussian Schell-model source to explore this effect further.

4. 1D GAUSSIAN SCHELL-MODEL SOURCE

As an example, we study the one-dimensional Gaussian Schell-model source because it is a well-studied representative of partially coherent fields; its extent in both space and frequency is cleanly described by two parameters, and its intensity profile is always a Gaussian. Its mutual intensity, Wigner distribution, and ambiguity function are all Gaussian functions as well. Furthermore, since the Gaussian achieves the uncertainty principle's minimum bound on the product of the variance of position and frequency, we expect that an analysis of the Gaussian Schell-model source should yield a conservative estimate for the effect of apodization on the ambiguity function, as apodization is more pronounced when farther away from the origin. A summary of functions, variables and coordinates to be used in the derivation is given in Table 1.

The (normalized) mutual intensity of the one-dimensional Gaussian Schell-model source in mean and difference coordinates is given by

$$\breve{J}(x, \xi) = \frac{1}{\sqrt{2\pi\sigma_I^2}} \exp[-x^2/(2\sigma_I^2)] \exp\left[-\xi^2\left(\frac{1}{8\sigma_I^2} + \frac{1}{2\sigma_\mu^2}\right)\right],$$

with parameters σ_I and σ_μ defined as they are in [12]. Hence, the ambiguity function for such a source is

$$A(f_x, \xi) = \exp(-2\pi^2 \sigma_I^2 f_x^2) \exp\left[-\xi^2\left(\frac{1}{8\sigma_I^2} + \frac{1}{2\sigma_\mu^2}\right)\right].$$

Table 1. Summary of Functions, Variables, and Coordinates Used in the Theoretical Derivation

$J(x_1, x_2)$	Mutual intensity function
$\breve{J}(x, \xi)$	Mutual intensity function written in mean (x) and difference (ξ) coordinates
$A(f_x, \xi)$	Ambiguity function ($x \leftrightarrow f_x$ is a Fourier pair)
$\mathcal{M}$	Overall degree of coherence
$\Pi(f_x, \xi)$	Apodization function
$\widetilde{A}(f_x, \xi)$	Apodized ambiguity function due to ignoring integration across pixel extent
$\widetilde{\mathcal{M}}$	Overall degree of coherence after apodization
$\widetilde{f}_x, \widetilde{\xi}$	Rescaled ambiguity function coordinates
$\widetilde{\Pi}(\widetilde{f}_x, \widetilde{\xi})$	Apodization function in rescaled coordinates
ρ, θ	Polar form of rescaled coordinates
γ	Helper variable for integration

The overall degree of coherence can be computed via Eq. (3):

$$\mathcal{M} = \iint \exp(-4\pi^2 \sigma_I^2 f_x^2) \exp\left[-\xi^2\left(\frac{1}{4\sigma_I^2} + \frac{1}{\sigma_\mu^2}\right)\right] df_x d\xi$$

$$= \frac{1}{2\sigma_I \sqrt{\pi}} \frac{2\sigma_I \sigma_\mu \sqrt{\pi}}{\sqrt{4\sigma_I^2 + \sigma_\mu^2}} = \frac{\sigma_\mu}{\sqrt{4\sigma_I^2 + \sigma_\mu^2}}.$$

This leads to a simpler expression for the ambiguity function:

$$A(f_x, \xi) = \exp(-2\pi^2 \sigma_I^2 f_x^2) \exp[-\xi^2/(8\sigma_I^2 \mathcal{M}^2)],$$

where one can view $\mathcal{M}$ as a parameter that simply adjusts the extent of the ambiguity function along ξ.

A. Theoretical Derivation for Noiseless Measurements

We consider an ideal phase space tomography procedure wherein the judicious, if not altogether practical, use of lenses allows us to measure each slice of the ambiguity function with a magnification factor of our choosing. While many practical measurement protocols have been proposed in the literature [2,5–7,13,14], we study our simpler model in order to glean an intuitive understanding free from distractions. More specifically, we will use the same full fill-factor imaging sensor for each image we capture, and we will adjust the magnification so that the Gaussian profile of the Schell-model source occupies the same extent on the imaging sensor for every angle in phase space. This results in the ratio of the pixel size to the Gaussian profile's width (i.e., standard deviation) being a constant, which we will define as φ. With this choice of magnification, the expression in Eq. (4) for the reduced overall degree of coherence $\widetilde{\mathcal{M}}$ can be simplified to

$$\widetilde{\mathcal{M}} = \mathcal{M} \iint \exp[-\pi(\widetilde{f}_x^2 + \widetilde{\xi}^2)]\widetilde{\Pi}^2(\widetilde{f}_x, \widetilde{\xi}) d\widetilde{f}_x d\widetilde{\xi}$$

via new coordinates $\widetilde{f}_x = (2\sigma_I \sqrt{\pi}) f_x$ and $\widetilde{\xi} = \xi/(2\sigma_I \mathcal{M} \sqrt{\pi})$. With this new coordinate system, the ambiguity function is rotationally symmetric, and thus the function $\widetilde{\Pi}$ must also be rotationally symmetric through our choice of magnification. We can thus write the ratio of the apparent overall degree of coherence to the true overall degree of coherence in terms of an integral in polar coordinates:

$$\widetilde{\mathcal{M}}/\mathcal{M} = \int_0^{2\pi} \int_0^\infty \exp(-\pi\rho^2) \frac{\sin^2(\sqrt{\pi}\varphi\rho/2)}{\pi\varphi^2\rho^2/4} \rho \, d\rho \, d\theta, \quad \textbf{(6)}$$

with polar coordinates defined by $\widetilde{f}_x = \rho \cos\theta$ and $\widetilde{\xi} = \rho \sin\theta$. By substituting $\sin^2(\sqrt{\pi}\varphi\rho/2)/\rho = \int_0^{\sqrt{\pi}\varphi/2} \sin(2\gamma\rho) d\gamma$, we can further simplify Eq. (6) to

$$\widetilde{\mathcal{M}}/\mathcal{M} = \frac{4}{\varphi^2} \int_0^{\sqrt{\pi}\varphi/2} \exp(-\gamma^2/\pi) \mathrm{erfi}(\gamma/\sqrt{\pi}) d\gamma$$

$$= {}_2F_2\left(1, 1; \frac{3}{2}, 2; -\varphi^2/4\right)$$

$$= \sum_{n=0}^\infty \frac{(-1)^n (\varphi)^{2n} \Gamma\left(\frac{3}{2}\right)}{4^n (n+1) \Gamma\left(n + \frac{3}{2}\right)},$$

where erfi is the imaginary error function, ${}_2F_2$ is a generalized hypergeometric function, and Γ is Euler's gamma function.

In practical situations, φ will be small, so it would be useful to expand the series for the first few coefficients:

$$\widetilde{\mathcal{M}}/\mathcal{M} = 1 - \frac{\varphi^2}{12} + \frac{\varphi^4}{180} - \frac{\varphi^6}{3360} + O(\varphi^8).$$

For small pixels where $\varphi \leq 1$, the quadratic term dominates the apparent fractional loss in overall degree of coherence. Thus, halving the pixel size results in quartering the apparent fractional loss. For pixels of size $\varphi = 1$, treating the noiseless pixel values as point measurements of the intensity results in reconstructing an overall degree of coherence that is approximately 92.2% of the true overall degree of coherence or 7.8% loss. For $\varphi = \frac{1}{2}$, this increases to 98.0% or 2.0% loss. A graph of $\widetilde{\mathcal{M}}/\mathcal{M}$ as a function of φ is shown in Fig. 1. We can use a similar derivation to compute the systematic relative error:

$$\mathcal{E} = \left[1 + \widetilde{\mathcal{M}}/\mathcal{M} - \frac{4\sqrt{\pi}}{\varphi} \exp(-\varphi^2/16)\mathrm{erfi}(\varphi/4)\right]^{1/2},$$

which is plotted in Fig. 2. For $\varphi = 1$, the systematic relative error is $\mathcal{E} = 5.68\%$, and for $\varphi = \frac{1}{2}$ the systematic relative error is $\mathcal{E} = 1.46\%$.

One way to interpret these results is to consider how much error one is willing to tolerate (or must tolerate due to noise) in the reconstructed overall degree of coherence (or likewise, the amount of error in the reconstructed mutual intensity) and use these equations and graphs to determine what is the largest pixel size that would be reasonable. For sources that are not Gaussian Schell-model sources, a good approximation would be to consider the second moment of the average power spectral density measured in each image and compute φ using the σ_I for a Gaussian Schell-model source with the same second moment.

B. Simulation Results for Noisy Measurements

In practice, noise as well as positivity constraints during reconstruction will also affect the quality of the reconstructed partially coherent field. Deriving a closed-form solution that also accounts for these aspects is difficult, so we instead opt for a numerical approach. We simulate a specific Gaussian Schell-model source being measured with two different sensor
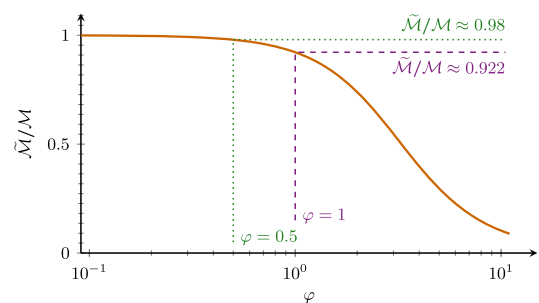

Fig. 1. Effect of pixel size on the reconstructed overall degree of coherence if pixel values were interpreted as point samples of the intensity. The horizontal axis gives the ratio (φ) of the pixel size to the standard deviation of the Gaussian intensity profile, and the vertical axis gives the ratio of the reconstructed overall degree of coherence ($\widetilde{\mathcal{M}}$) to the true overall degree of coherence ($\mathcal{M}$) assuming noiseless measurements.
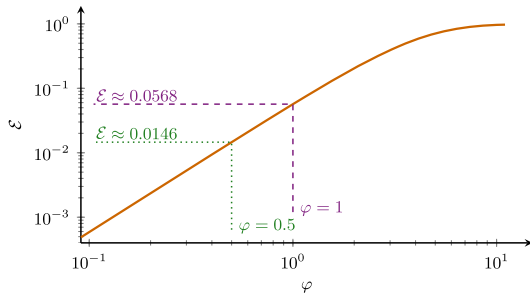
Fig. 2. Systematic relative error introduced to the reconstructed mutual intensity if pixel values were interpreted as point samples of the intensity. The horizontal axis gives the ratio (φ) of the pixel size to the standard deviation of the Gaussian intensity profile, and the vertical axis gives the relative error ($\mathcal{E}$) defined in Eq. (5).

Fig. 3. Contour plot of the magnitude of the theoretical ground truth mutual intensity function near the origin.

configurations subject to varying amounts and types of noise; the mutual intensity is then reconstructed from these measurements to determine the resulting overall degree of coherence as well as relative reconstruction error. We chose a source with the following parameters:

$$\lambda = 632.8 \text{ nm}, \qquad \sigma_I = 8 \text{ μm}, \quad \text{and} \quad \sigma_\mu = 16 \text{ μm}.$$

For numerical computation, we discretized the mutual intensity into a 101×101 matrix using a spatial sinc basis with a sampling interval equal to 2 μm. We found that this discretization was sufficient to describe the mutual intensity up to machine precision.

We chose two sensor configurations—101 pixels spaced 4 μm apart and 51 pixels spaced 8 μm apart, corresponding to $\varphi = \frac{1}{2}$ and $\varphi = 1$, respectively. The distance between the first pixel and the last pixel is thus constant in both configurations, making pixel pitch the main difference between the two configurations. Intensity measurements covered 100 different slices of the ambiguity function, spaced evenly in θ as per the coordinate system used in Eq. (6). The magnification per slice was adjusted so that the Gaussian intensity profile falling on the sensor was always the same width as the width at $\theta = 0$. In practice, this would be implemented using a lens system, but here we assume a perfect imaging system for simplicity and to isolate sources of error for better understanding of the results.

The noiseless pixel values were computed using closed-form integration of the Gaussian function across the extents of the pixels. We simulated eight different levels of primarily two different types of noise: Gaussian and Poisson. For Gaussian noise, we added to each noiseless pixel value a Gaussian random value with standard deviation equal to $\sigma_{\text{rel}}I_{\text{max}}$, where I_{max} is the highest noiseless pixel value, and σ_{rel} took on values exponentially evenly spaced between $10^{-4.5}$ and 10^{-1}; this corresponded to capturing noisy images with peak signal-to-noise ratios (PSNRs) evenly spaced between 20 dB and 90 dB. We follow the standard imaging processing literature (see, e.g., [15]) by defining PSNR as $20 \log_{10}(I_{\text{max}}/\sigma_{\text{error}})$, where σ_{error} is the standard deviation of the error in intensity, which is proportional to pixel value. For Poisson noise, we considered total photon counts exponentially evenly spaced between 10^3 and 10^{10}. Each noisy pixel measurement was generated by
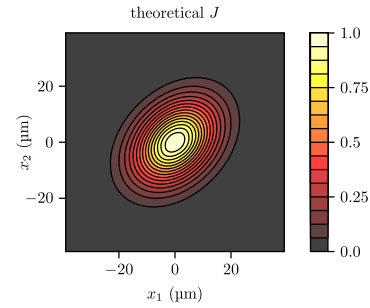
drawing from a Poisson distribution with the rate parameter proportional to the intensity. The rate parameters were scaled such that their sum was equal to the total photon count.

For each sensor configuration, noise type, and noise level, we created 20 data sets of noisy measured pixel values. With each data set, we first ran a nonnegative-constrained coherence retrieval algorithm [16] using a "point sample" forward operator that assumed the pixel values to be point samples of the intensity. Then, to determine the effect of pixel integration, we used the same algorithm but with a different "pixel-integrated" forward operator that took into account integration across the pixel (numerically simulated as taking the intensity at 256 evenly spaced positions covering the extent of the pixel). The details of the two forward operators as well as algorithm-specific parameters are given in Appendix A.

A contour plot of the magnitude of the theoretical (ground truth) mutual intensity function near the origin is given in Fig. 3. For one instance (i.e., data set) of Gaussian noise at PSNR = 50 dB, we give contour plots for the reconstructed mutual intensity functions with the two different forward operators in Fig. 4 for the $\varphi = \frac{1}{2}$ case. Similar plots are shown for one instance of the $\varphi = 1$ case in Fig. 5. For Gaussian noise, a plot of the reconstructed overall degree of coherence as a function of noise level and forward operator is given in Fig. 6 for both values of φ. A similar plot of relative error is given in Fig. 7. Corresponding plots for Poisson noise are given in Figs. 8 and 9, with plots for a mixture of noise types given in Appendix B.

These plots first validate our theoretical results for the noiseless case, as the apparent loss in coherence and reconstruction
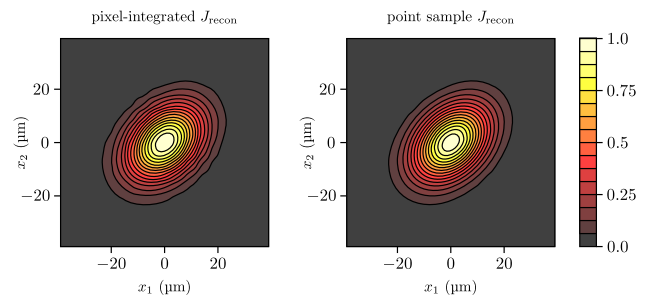

Fig. 4. Contour plots for the reconstructed mutual intensity function given measurement PSNR = 50 dB for both pixel-integrated (left) and point sample (right) forward operators when $\varphi = \frac{1}{2}$.
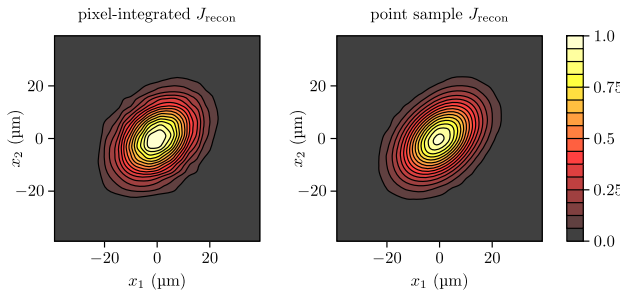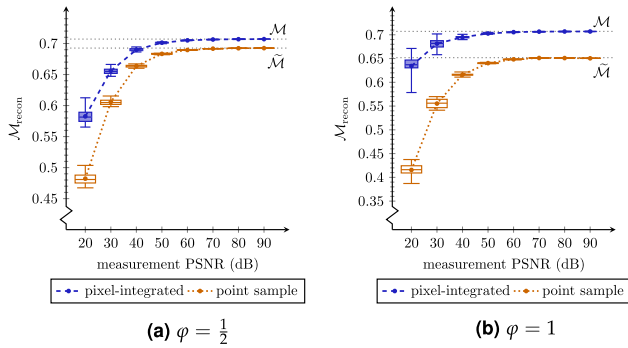
Fig. 5. Contour plots for the reconstructed mutual intensity function given measurement PSNR = 50 dB for both pixel-integrated (left) and point sample (right) forward operators when $\varphi = 1$.

Fig. 8. Box plots of the reconstructed overall degree of coherence $\mathcal{M}_{\text{recon}}$ as a function of the total photon count for Poisson noise.

Fig. 6. Box plots of the reconstructed overall degree of coherence $\mathcal{M}_{\text{recon}}$ as a function of the measurement PSNR for Gaussian noise. The top and bottom whiskers give the maximum and minimum, and the box gives the first and third quartiles in addition to the median, with the mean plotted using circular markers. Dotted horizontal lines give theoretical values computed in the previous section. "Pixel-integrated" results use narrow filled boxes with navy dashed lines connecting the means, and "point sample" results use wide outlined boxes with tan/dotted lines connecting the means.

error for the point-intensity forward operator converge toward the values predicted in the previous section as noise levels approach zero (i.e., as the measurement PSNR and photon counts increase). This convergence makes it apparent that
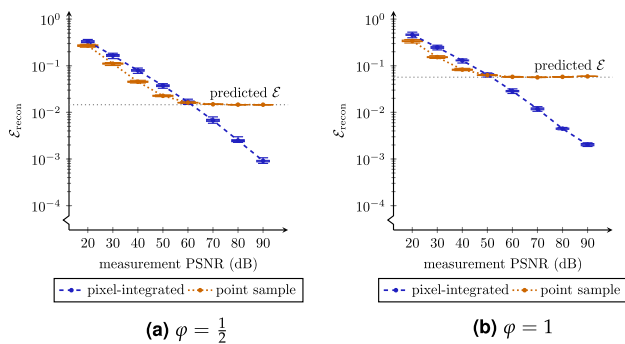

Fig. 7. Box plots of the reconstruction (relative) error $\mathcal{E}_{\text{recon}}$ as a function of the measurement PSNR for Gaussian noise. The dotted horizontal lines give the systematic relative error computed in the previous section.
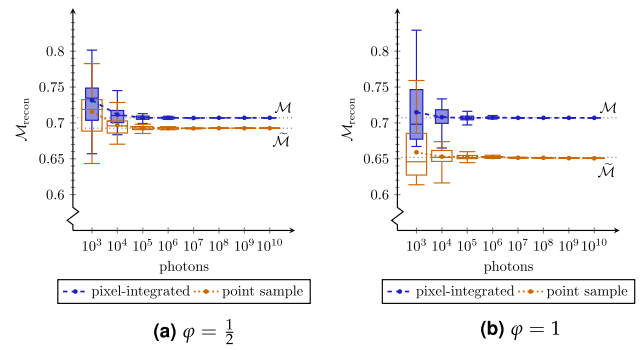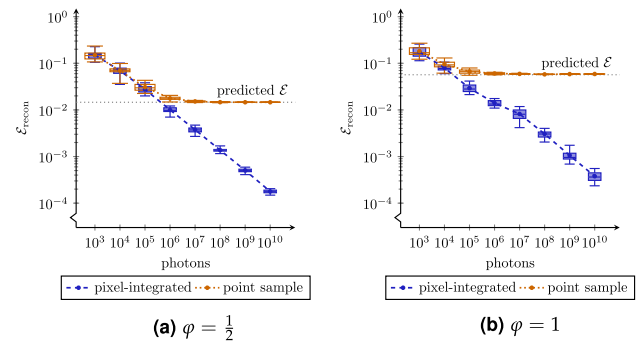

Fig. 9. Box plots of the reconstruction (relative) error $\mathcal{E}_{\text{recon}}$ as a function of the total photon count for Poisson noise.

the dominating factor for the drop in apparent coherence at lower noise levels is due to pixel integration.

As measurement PSNR decreases, however, noise becomes the dominant factor in both apparent coherence loss and reconstruction error. For $\varphi = \frac{1}{2}$, noise becomes the dominant factor below a measurement PSNR of 60 dB, whereas the threshold is 50 dB for $\varphi = 1$. This is quite apparent in Fig. 5, where the pixel-integrated reconstruction maintains its width but is quite noisy compared to the point sample reconstruction, which is skinnier but smoother. The same can be seen in the Poisson noise results, where the threshold appears to be between 10^5 and 10^6 photons for the $\varphi = \frac{1}{2}$ case and between 10^4 and 10^5 photons for the $\varphi = 1$ case. In fact, at noise levels beyond these thresholds, using a forward operator that takes into account pixel integration actually performs slightly *worse* in terms of relative error, even though the recovered overall degree of coherence is closer to the ground truth. This is especially apparent in the Gaussian noise case. We hypothesize that this is due to the pixel-integrated forward operator being more ill-posed since we are effectively performing a phase space deconvolution when reconstructing the mutual intensity.

These results suggest that for accurate estimation of the overall degree of coherence as well as accurate reconstruction of the mutual intensity, the reconstruction algorithm should ideally take integration across a pixel into account. However, in situations of high noise, the noise itself will be the primary

limiting factor and thus a simpler reconstruction scheme based on the point-sampled intensity assumption may be sufficient. For more accurate reconstruction, even in the presence of high noise levels, we may be able to achieve better results by the judicious use of a regularizer with a forward operator that includes integration across a pixel's extent. Further study into the choice of regularizer is a promising route for future work.

APPENDIX A: NUMERICAL RECONSTRUCTION PROCESS

We perform numerical reconstruction of the mutual intensity from noisy intensity measurements via the following positive semidefinite least squares problem:

$$\underset{X}{\text{minimize}} \; \frac{1}{2}\|\mathcal{A}(X) - b\|_2^2 \text{ subject to } X \succeq 0,$$

where X is an intermediate representation of the mutual intensity, while $\mathcal{A}$ and b are the weighted forward operator and weighted noisy measurements, respectively. The mth element of b is equal to $b_m = y_m/\sigma_m$, where y_m is the mth measurement, and σ_m is the noise standard deviation of the mth measurement.

1. Mutual Intensity Representation

The mutual intensity matrix J is related to X via

$$J = PXP^{\mathrm{H}},$$

where P is a basis preconditioner whose derivation we will discuss later. For the Gaussian Schell-model source described in Section 4, J is a 101 × 101 matrix given by

$$J = \begin{pmatrix} J_{-50,-50} & J_{-50,-49} & \cdots & J_{-50,50} \\ J_{-49,-50} & J_{-49,-49} & \cdots & J_{-49,50} \\ \vdots & \vdots & \ddots & \vdots \\ J_{50,-50} & J_{50,-49} & \cdots & J_{50,50} \end{pmatrix}.$$

The entries of the mutual intensity matrix give the coefficients for a discretization of the mutual intensity function via a sinc basis:

$$J(x_1, x_2) = \sum_{k,l} J_{k,l} \operatorname{sinc}[(x_1 - k\Delta_s)/\Delta_s]\operatorname{sinc}[(x_2 - l\Delta_s)/\Delta_s],$$

where $\operatorname{sinc} x = \sin(\pi x)/(\pi x)$. The ground truth mutual intensity matrix, computed via numerical integration in MATLAB, is given by

$$J_{k,l}^{\text{true}} = 2\sigma_I \mathcal{M}\sqrt{2\pi} \iint \operatorname{rect}(\Delta_s f_1)$$
$$\times \operatorname{rect}(\Delta_s f_2)s_{k,l}(f_1, f_2)\mathrm{d}f_1\mathrm{d}f_2,$$

where

$$s_{k,l}(f_1, f_2) = \exp[-\mathrm{j}2\pi\Delta_s(f_1 k + f_2 l)]$$
$$\times \exp\{-2\pi^2\sigma_I^2[(f_1 + y_2)^2 + \mathcal{M}^2(f_1 - f_2)^2]\}.$$

2. Forward Operator

The mth output element of the operator $\mathcal{A}$ is given by

$$\mathcal{A}[m](X) = \operatorname{tr}(K_m PXP^{\mathrm{H}})/\sigma_m, \qquad \textbf{(A1)}$$

where K_m is a matrix that describes how one obtains the mth noiseless intensity measurement from the mutual intensity

matrix J. The forward operator that assumes the pixel values to be point samples is given by

$$K_m^{(1)} = \Delta_x k(x_m, \theta_m)k^H(x_m, \theta_m),$$

whereas a forward operator that takes into account pixel integration is given by

$$K_m^{(p)} = \int_{x_m - \Delta_x/2}^{x_m + \Delta_x/2} k(\xi, \theta_m)k^{\mathrm{H}}(\xi, \theta_m)\mathrm{d}\xi$$

$$\approx \sum_{p=1}^{256} \widetilde{\Delta}_x k(x_m + p\widetilde{\Delta}_x - \gamma, \theta_m)k^{\mathrm{H}}(x_m + p\widetilde{\Delta}_x - \gamma, \theta_m),$$

where $\gamma = \dfrac{257}{2}\widetilde{\Delta}_x$, $\quad \widetilde{\Delta}_x = \Delta_x/256$.

For both operators, θ_m is the rotation angle in ambiguity function space:

$$\theta_m \in \{-\pi/2, \pi/100 - \pi/2, \ldots, \pi/2 - \pi/100\},$$

where x_m gives the pixel centers for both operators, and Δ_x gives the pixel spacing (and width for the integrated case). For pixel size corresponding to $\varphi = \frac{1}{2}$, we set

$$x_m/\Delta_x \in \{-50, -49, \ldots, 50\}, \quad \text{with } \Delta_x = 4 \text{ μm},$$

whereas for the $\varphi = 1$ case, we have

$$x_m/\Delta_x \in \{-25, -24, \ldots, 25\}, \quad \text{with } \Delta_x = 8 \text{ μm}.$$

The vector-valued coherent forward operator function $k(x, \theta)$ is derived via the transmission function [17] or the amplitude spread function [18]:

$$k(x, \theta) = (\, k_{-50}(x, \theta) \quad k_{-49}(x, \theta) \quad \cdots \quad k_{50}(x, \theta)\,)^{\mathrm{T}},$$

where

$$k_l(x, \theta) = k_l^{(\text{fresnel})}\left[x\sqrt{1 + \tan^2\theta}, \sigma_\xi \tan\theta/(\sigma_{f_x}\lambda)\right],$$

and for the special case of $\theta = \pm\pi/2$,

$$k_l(x, \pm\pi/2) = \exp(\mp\mathrm{j}2\pi\Delta_s lx\sigma_{f_x}/\sigma_\xi)\sqrt{\Delta_s\sigma_{f_x}/\sigma_\xi}.$$

$k_l^{(\text{fresnel})}(r, z)$ is the coherent field as a function of r that the lth sinc basis function induces at a propagation distance of z, arrived via the Fresnel diffraction integral:

$$k_l^{(\text{fresnel})}(r, z)$$
$$= \frac{\exp[\alpha_{lrz}]}{2\sqrt{\mathrm{j}\lambda z/\Delta_s}}\{\operatorname{erf}[-\sqrt{\alpha_{lrz}} + \beta_z] - \operatorname{erf}[-\sqrt{\alpha_{lrz}} - \beta_z]\},$$

where $\alpha_{lrz} = \mathrm{j}\pi(r - l\Delta_s)^2/(\lambda z)$, $\beta_z = \dfrac{\sqrt{\mathrm{j}\pi\lambda z}}{2\Delta_s}$, and $\sqrt{\mathrm{j}} = (1 + \mathrm{j})/\sqrt{2}$.

In practice, the K_ms would be expensive to store in their exact form, so we store a rank-12 approximation instead, i.e.,

$$K_m \approx \widetilde{K}_m\widetilde{K}_m^H, \quad \text{with } \widetilde{K}_m^{(1)} \in \mathbb{C}^{101\times1}, \quad \text{and}$$
$$\widetilde{K}_m^{(p)} \in \mathbb{C}^{101\times12},$$

since we found empirically for this forward operator that all of the K_ms had insignificant eigenvalues after the 12th one.

3. Basis Preconditioning

We found that without preconditioning (i.e., $P = I$) convergence was slow. This was due to the fact that a large spread in the σ_ms, especially in the Poisson noise case, caused $\mathcal{A}$ to be severely ill-conditioned. In the worst case, we found that certain combinations of basis functions in the mutual intensity converged much more slowly than other combinations. An *ad hoc* remedy we adopted was the following. We first write

$$A = \begin{pmatrix} \widetilde{K}_1 & \widetilde{K}_2 & \cdots & \widetilde{K}_M \end{pmatrix} = U_A \Sigma_A V_A^H,$$

and then we set $P = U_A \Sigma_A^{-1} U_A^H$. This induces a new nonnormalized basis such that

$$\sum_m P K_m P^H = I.$$

This preconditioning effectively enforces a conservation of energy rule on the weighted forward operator—an increase in the trace of X results in the exact same increase in the sum of the entries of $\mathcal{A}(X)$. We found that using such a preconditioner sped up our reconstruction process by many orders of magnitude in some extreme cases. A deeper look into the design of this preconditioner may be a good topic for future study.

4. Numerical Algorithm

We solved Eq. (A1) using the algorithm given in [16], running the algorithm for at most 1000 iterations with each set of noisy data and standard options. The algorithms took several minutes per set of measurements for the point-sampled forward operator and up to 1 h for the pixel-integrated forward operator on two cores of a Xeon E7-4850 2 GHz processor running MATLAB.

APPENDIX B: MIXTURE OF POISSON AND GAUSSIAN NOISE

We also considered a scenario where Gaussian noise was added to Poisson noise, as this would be a more realistic scenario. The noisy measurements at the nth noise level were generated by adding Gaussian noise at the nth measurement PSNR to a noisy Poisson measurement corresponding to the nth photon count. However, the results shown in Figs. 10 and 11 look very
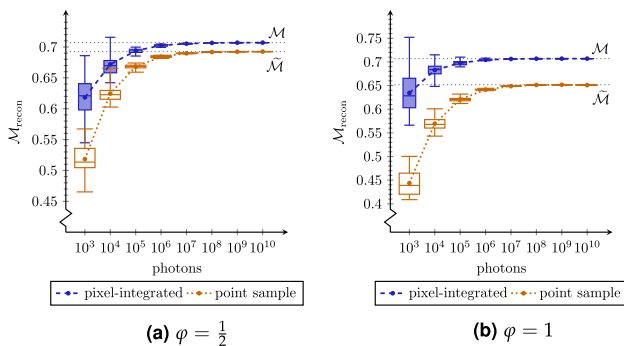
Fig. 10. Box plots of the reconstructed overall degree of coherence $\mathcal{M}_{\text{recon}}$ as a function of the total photon count. A similar level of Gaussian noise was also added to the measurements.
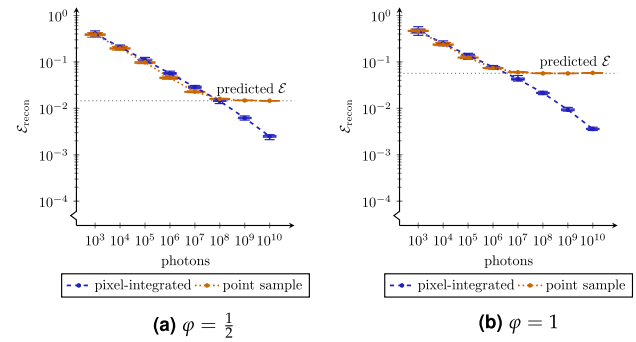
Fig. 11. Box plots of the reconstruction (relative) error $\mathcal{E}_{\text{recon}}$ as a function of the total photon count. A similar level of Gaussian noise was also added to the measurements.

similar to something halfway between the results for Gaussian and Poisson noise alone.

REFERENCES

1. M. G. Raymer, M. Beck, and D. McAlister, "Complex wave-field reconstruction using phase-space tomography," Phys. Rev. Lett. **72**, 1137–1140 (1994).
2. D. F. McAlister, M. Beck, L. Clarke, A. Mayer, and M. G. Raymer, "Optical phase retrieval by phase-space tomography and fractional-order Fourier transforms," Opt. Lett. **20**, 1181–1183 (1995).
3. M. Ježek and Z. Hradil, "Reconstruction of spatial, phase, and coherence properties of light," J. Opt. Soc. Am. A **21**, 1407–1416 (2004).
4. C. Rydberg and J. Bengtsson, "Numerical algorithm for the retrieval of spatial coherence properties of partially coherent beams from transverse intensity measurements," Opt. Express **15**, 13613–13623 (2007).
5. L. Tian, J. Lee, S. B. Oh, and G. Barbastathis, "Experimental compressive phase space tomography," Opt. Express **20**, 8296–8308 (2012).
6. Z. Zhang, Z. Chen, S. Rehman, and G. Barbastathis, "Factored form descent: a practical algorithm for coherence retrieval," Opt. Express **21**, 5759–5780 (2013).
7. A. Cámara, J. A. Rodrigo, and T. Alieva, "Optical coherenscopy based on phase-space tomography," Opt. Express **21**, 13169–13183 (2013).
8. A. Papoulis, "Ambiguity function in Fourier optics," J. Opt. Soc. Am. **64**, 779–788 (1974).
9. K.-H. Brenner and J. Ojeda-Castañeda, "Ambiguity function and Wigner distribution function applied to partially coherent imagery," J. Mod. Opt. **31**, 213–223 (1984).
10. M. J. Bastiaans, "The Wigner distribution function of partially coherent light," Opt. Acta **28**, 1215–1224 (1981).
11. E. Wolf, "New theory of partial coherence in the space-frequency domain. Part I: spectra and cross spectra of steady-state sources," J. Opt. Soc. Am. **72**, 343–351 (1982).

12. A. Starikov and E. Wolf, "Coherent-mode representation of Gaussian Schell-model sources and of their radiation fields," J. Opt. Soc. Am. **72**, 923–928 (1982).

13. D. M. Marks, R. A. Stack, and D. J. Brady, "Astigmatic coherence sensor for digital imaging," Opt. Lett. **25**, 1726–1728 (2000).

14. A. Cámara, T. Alieva, I. Castro, and J. A. Rodrigo, "Phase-space tomography for characterization of rotationally symmetric beams," J. Opt. **16**, 015705 (2014).

15. R. Szeliski, *Computer Vision: Algorithms and Applications* (Springer, 2010).

16. C. Bao, G. Barbastathis, H. Ji, Z. Shen, and Z. Zhang, "A trace-regularized method for coherence retrieval," arXiv:1706.03963v1 (2017).

17. M. Born and E. Wolf, *Principles of Optics*, 7th ed. (Cambridge University, 2005).

18. J. W. Goodman, *Statistical Optics* (Wiley, 1985).